WEP Warwick Evans Publishing

International Journal of Mechanical and Electrical Engineering

ISSN: 3005-9615 (Print), ISSN: 3005-7132 (Online) | Volume 8, Number 5, Year 2026
DOI: https://doi.org/10.62051/ijmee.v8n5.02
Journal homepage: https://wepub.org/index.php/IJMEE/index

Asperity-Coupled Flash Heating, Stress Oscillation, and Synergistic Plastic Dissipation in Dual-Roughness Disc-Pad Brake Interfaces

Pengfei Cui [1, 2], Liangbi Wang [1, 2]

[1] School of Mechatronic Engineering, Lanzhou Jiaotong University, Lanzhou Gansu, 730070, China

[2] Key Laboratory of Railway Vehicle Thermal Engineering, Ministry of Education, Lanzhou Gansu, 730070, China

ABSTRACT

To investigate the local flash temperature, stress oscillations, and elastoplastic energy dissipation induced by asperity interactions on both sides of a high-speed train disc brake, a three-dimensional transient thermo-mechanically coupled finite element model of a dual-roughness disc-pad interface was established. A fixed Weierstrass-Mandelbrot fractal morphology was used to evaluate temperature, von Mises stress, thermal penetration depth, thermoelastic power, plastic dissipation, and frequency-domain responses. The peak temperatures of the brake disc and brake pad reached 1409.5 °C and 1571.9 °C, respectively, and the corresponding peak von Mises stresses were 1079.4 MPa and 1024.6 MPa. The dominant stress frequency was 3395.6 Hz, with a relative oscillation amplitude of 312.10%. Plastic power accounted for approximately 32% and 37% of the theoretical input power in the disc and pad, respectively. Misaligned asperity contact and repeated jumps in contact stiffness jointly caused near-surface heat accumulation, high-frequency instability, and synergistic plastic dissipation.

KEYWORDS

High-speed Train Disc Brake; Dual-roughness Interface; Thermo-mechanical Coupling; Elastoplastic Energy Dissipation; Thermal Instability.

1. INTRODUCTION

During emergency braking or braking on long steep grades, high-speed train disc brakes are subjected to short-duration, high-power frictional input. Frictional heat generation, heat diffusion, thermal expansion, contact stress redistribution, and elastoplastic deformation occur simultaneously at the contact interface between the brake disc and the brake pad. If local heat cannot diffuse in time, flash temperature, hot spots, and thermal stress concentration readily form at the interface, further inducing thermal cracks, aggravated wear, friction-induced vibration, and even thermal instability. [1–3] Therefore, accurately describing the contact behavior of rough asperities at the braking interface is fundamental for explaining brake surface temperature and heat generated by elastoplastic deformation. [4,5]

The actual surfaces of brake discs and pads are composed of asperities whose heights, curvatures, and spatial distributions are stochastic. The real contact area is usually far smaller than the nominal contact area, and load and heat flux can be transmitted only through a limited number of contact patches. [4,6] Existing rough-contact studies often idealize one surface as smooth, making it difficult to describe sudden changes in contact stiffness caused by misalignment, collision, compaction, and

separation of asperities on both sides, and also difficult to characterize the energy allocation process when plastic dissipation occurs simultaneously in the brake disc and the brake pad. [5]

To reveal the interfacial response when rough morphologies on both sides jointly participate in load bearing and heat transfer, this paper establishes a three-dimensional transient thermo-mechanically coupled finite element model in which both the brake disc and the brake pad contain local rough bodies. Under a unified fractal morphology and fixed operating conditions, the surface temperature, von Mises stress, temperature attenuation along the depth direction, thermoelastic power, and plastic dissipation power on both sides are analyzed, and interfacial thermal instability is characterized using time-domain and frequency-domain indicators.

This paper focuses on three interrelated issues: how the dynamic migration of bilateral asperity contact patches changes local heat-flux density and peak stress; how frictional heat, thermoelastic effects, and plastic dissipation are distributed in the surface and subsurface layers; and how repeated transitions in contact stiffness trigger high-frequency stress oscillations. By incorporating geometrical morphology, material nonlinearity, and energy dissipation into a unified computational framework, the instability mechanism of the dual-roughness interface can be interpreted from the three aspects of heat transfer, mechanical response, and energy conversion.

2. NUMERICAL MODEL AND METHOD

2.1. Geometric Model and Rough Surfaces

The computational model consists of a sector-shaped brake disc and a brake pad. The outer radius, inner radius, and thickness of the brake disc are 370 mm, 220 mm, and 20 mm, respectively; the outer radius and thickness of the brake pad are 360 mm and 14 mm, respectively. To balance computational efficiency and local contact accuracy, local rough bodies are arranged only in the frictional contact region. The rough body on the brake-disc side has dimensions of 5 mm × 5 mm × 1 mm, and that on the brake-pad side has dimensions of 8×8×1 mm3. A 50° sector of the disc is used, and periodic boundary conditions are applied to ensure displacement and temperature continuity on the two sides of the sector.

This local modeling strategy preserves the main geometrical and kinematic relationships of the brake disc-pad contact while avoiding the enormous computational cost of discretizing the entire disc and pad with micrometer-scale meshes. Transition meshes are arranged between the local rough bodies and the main structures so that the temperature and stress gradients near the contact patches can be captured in detail, whereas a lower mesh density is maintained away from the contact zone. Displacement constraints are applied to the inner-radius cylindrical surface and the bottom surface of the brake disc, a uniformly distributed normal load is applied to the upper surface of the brake pad, and a Coulomb friction model is adopted at the contact interface. Through this boundary treatment, the model can simulate local sliding contact during disc rotation while ensuring mechanical and thermal continuity of the computational domain.

The rough surfaces are generated using the Weierstrass-Mandelbrot (W-M) fractal function. This method can superpose a finite number of frequency components to generate a random rough surface with self-similar characteristics. By fixing the random phases, exactly the same surface morphology is used in different simulation cases, thereby isolating the influence of geometrical randomness on the results. The two-dimensional W-M fractal surface can be written as:

$$z(x,y) = L\left(\frac{G}{L}\right)^{D-2}\left(\frac{\ln\gamma}{M}\right)^{1/2} \sum_{m=1}^{M}\sum_{n=n_{\max}}^{n_{\max}} \gamma^{(D-3)n}\left\{\cos\phi_{m,n} - \cos\left[\frac{2\pi\gamma^{n}\sqrt{x^2+y^2}}{L}\cos\left(\tan^{-1}\left(\frac{y}{x}\right) - \frac{\pi m}{M}\right) + \phi_{m,n}\right]\right\} \tag{1}$$

where D is the fractal dimension, G is the fractal scaling coefficient, M is the number of superposed corrugations, $\varphi_{m,n}$ is a random phase between 0 and 2π, γ^n denotes the frequency, n_{max} represents the upper frequency limit, and L is the surface length. In this study, $D = 2.5$, $G = 3.0$, and $L = 500$ μm are adopted. Point clouds are first generated in MATLAB and then imported into modeling software to form three-dimensional rough bodies.

The fractal dimension and scaling coefficient determine the peak-valley fluctuation and spatial frequency distribution of the rough surface. After D, G, and the random seed are fixed, the rough surfaces on both sides remain consistent throughout all calculations, so that the temperature, stress, and energy responses can be attributed to contact evolution and material nonlinearity, avoiding the scatter caused by repeatedly generated random morphologies.

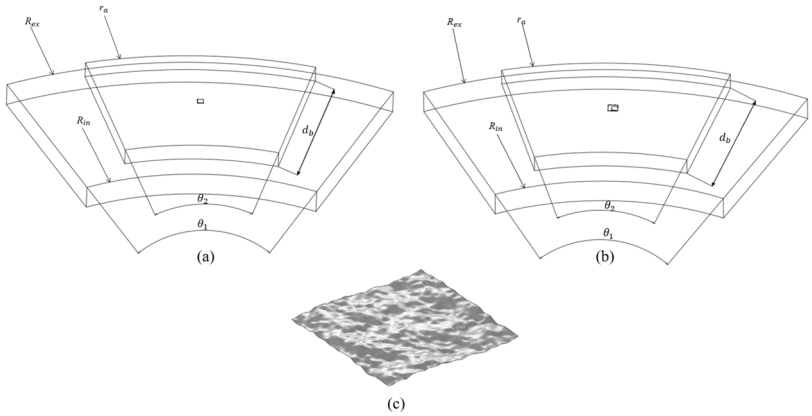

Figure 1. Dual-roughness contact geometry and W-M rough surface morphology

Table 1. Main model and computational parameters

Item	Brake disc	Brake pad/contact	Value or description
Material	Q345B	Copper-based powder metallurgy	Johnson-Cook elastoplastic damage model
Geometric dimensions	R_{out} = 370 mm; R_{in} = 220 mm; thickness = 20 mm	Outer radius = 360 mm; thickness = 14 mm	-
Local rough body	5 × 5 × 1 mm^3	8 × 8 × 1 mm^3	D = 2.5, G = 3.0, L = 500 μm
Load and motion	-	Normal pressure applied to the upper surface	16 kN, 48 rad/s, v = 14.16 m/s
Friction and time	-	μ = 0.4	Initial temperature 25 °C; duration 200 μs
Mesh	C3D8T; rough zone 40 μm	Thermally coupled tetrahedral elements; rough zone 10 μm	Approximately 1.77 million nodes and 1.50 million elements

2.2. Thermo-Mechanical Coupling Equations and Material Model

The brake assembly as a whole is treated as a small-deformation elastoplastic continuum. The initial temperature and ambient temperature are both 25 °C, and external heat sources are neglected. Frictional heat at the contact interface is jointly determined by relative sliding, normal contact pressure, and the friction coefficient; meanwhile, plastic work inside the material and thermoelastic effects provide additional contributions to the temperature field [5–7]. Under isotropic conditions, the transient heat-conduction governing equation can be written as:

$$\rho C_V \frac{\partial T}{\partial t} = k\nabla^2 T + \beta\boldsymbol{\sigma} : \dot{\boldsymbol{\varepsilon}}^p - \boldsymbol{D} : \alpha \boldsymbol{I} : \left(\dot{\boldsymbol{\varepsilon}} - \dot{\boldsymbol{\varepsilon}}^p\right) T + \mu p v \tag{2}$$

where ρ is the density, C_v is the specific heat at constant volume, k is the thermal conductivity, β is the Taylor-Quinney coefficient, σ is the stress tensor, ε^p is the plastic strain rate, α is the thermal expansion coefficient, D is the elastic tensor, κ is the heat partition coefficient, p is the local contact pressure, and v is the relative sliding velocity.

The first term on the right-hand side of the governing equation represents heat conduction, the second term represents irreversible dissipation caused by the conversion of plastic work into heat, the third term represents the thermoelastic coupling term, and the fourth term represents interfacial frictional heat input. For high-speed braking, the frictional heat source is usually the direct cause of near-surface temperature rise, whereas plastic dissipation determines irreversible heat generation and material damage in the subsurface layer. The thermoelastic term reflects the bidirectional conversion between temperature change and elastic strain energy, and therefore its sign may alternate between positive and negative over time.

During braking, the material undergoes an elastic stage, an elastoplastic yielding and hardening stage, and a damage-failure stage. Yielding is judged using the von Mises criterion and J_2 flow theory, and the equivalent stress is expressed as:

$$f = \bar{\sigma} - \sigma_y, \quad \bar{\sigma} = \sqrt{\frac{3}{2} s_{ij} s_{ij}} \tag{3}$$

In the plastic stage, the Johnson-Cook constitutive model is used to describe strain hardening, strain-rate sensitivity, and thermal softening:

$$\sigma_f = \left[A + B\left(\bar{\varepsilon}^{pl}\right)^n\right]\left[1 + C\ln\left(\frac{\dot{\bar{\varepsilon}}^{pl}}{\dot{\varepsilon}_0}\right)\right]\left[1 - \left(T^*\right)^m\right] \tag{4}$$

$$T^* = \frac{\left(T - T_0\right)}{\left(T_{melt} - T_0\right)} \tag{5}$$

where A, B, C, n, and m are material constants, ε^p is the equivalent plastic strain $\dot{\varepsilon}_0$ is the reference strain rate, and T_{melt} is the melting temperature. Damage initiation is described using the Johnson-Cook shear-failure criterion, and the failure strain is written as:

$$\bar{\varepsilon}_f^{pl} = \left[d_1 + d_2 \exp\left(d_3\eta\right)\right]\left[1 + d_4 \ln\frac{\dot{\bar{\boldsymbol{\varepsilon}}}^{pl}}{\dot{\boldsymbol{\varepsilon}}_0}\right]\left[1 + d_5\left(T^*\right)\right] \tag{6}$$

When the damage state variable continues to accumulate and exceeds the critical value, the element stiffness degrades according to the damage evolution law until element failure and deletion occur. This setting can reflect the influence of high temperature, strong shear, and accumulated plastic strain on the local contact state of the brake pad.

The brake disc material is Q345B, with parameters E = 208 GPa, ρ = 7850 kg/m³, k = 48 W/(m·K), $\alpha = 1.5 \times 10^{-5}$ K⁻¹, C_v = 611 J/(kg·K), and v = 0.31; the Johnson-Cook parameters are A = 382 MPa, B = 809 MPa, C = 0.019, n = 0.401, m = 0.432, and T_m = 1350 °C. The brake pad is made of a copper-based powder metallurgy material, with parameters E = 5.2 GPa, ρ = 5500 kg/m³, k = 30 W/(m·K), $\alpha = 2.24 \times 10^{-5}$ K⁻¹, C_v = 550 J/(kg·K), and v = 0.30; the Johnson-Cook parameters are A = 90 MPa, B = 292 MPa, C = 0.025, n = 0.31, m = 1.09, and T_m = 1524 °C. The thermal properties of the materials are treated as constants within the time scale of this calculation.

2.3. Finite Element Setup, Energy Indicators, and Validation

The finite element calculation is performed in ABAQUS/Explicit for three-dimensional transient thermo-mechanically coupled solution. The main body of the brake disc uses C3D8T eight-node thermally coupled hexahedral elements, while the brake pad and complex regions use thermally coupled tetrahedral elements. The mesh size in the rough zone is 40 μm on the brake-disc side and 100 μm on the brake-pad side, and transition meshes are arranged between the rough bodies and the main structures. A 16 kN normal load is applied to the upper surface of the brake pad, and the brake disc rotates at a constant angular velocity of 48 rad/s. The local sliding speed at the evaluation position is approximately 14.16 m/s; the friction coefficient is 0.4, and the calculation duration is 200 μs.

To quantify the allocation of frictional energy among different channels, the theoretical input power is defined as:

$$P_{input} = \frac{\mu p v}{A_{break}} \tag{7}$$

where v is the local sliding velocity. The plastic dissipation power and thermoelastic power are obtained by integrating state variables, and their ratios are defined as:

$$P_{input} = \frac{\mu p v}{A_{break}} \tag{8}$$

$$\eta_{plast} = \frac{\sum_{i=1}^{N}\left[\left(\boldsymbol{D}:\alpha \boldsymbol{I}:\left(\dot{\boldsymbol{\varepsilon}}-\dot{\boldsymbol{\varepsilon}}^{p}\right)T\right)_{i} dV_{i}\right]}{P_{input}\times A_{nominal}}\times 100\%, \eta_{elast} = \frac{\sum_{i=1}^{N}\left[\left(\beta\boldsymbol{\sigma}:\dot{\boldsymbol{\varepsilon}}^{p}\right)_{i} dV_{i}\right]}{P_{input}\times A_{nominal}}\times 100\% \tag{9}$$

Mesh independence is examined using the elastoplastic dissipation depth beneath the highest rough peak. Under different meshes, the curve evolution trends are consistent, and the maximum relative error is 4.68%, satisfying the requirement for local convergence. Meanwhile, the model captures patterns such as mechanical response preceding temperature response and plastic deformation concentrating in the subsurface layer, which are consistent with published experiments and classical rough-contact studies. This indicates that the model can reasonably capture the transient thermo-mechanical coupling process.

The result analysis selects the time interval during which the highest asperity makes primary contact with the counter surface. In this stage, the heat-source position is clear and the load is concentrated, making it suitable for identifying the initial evolution of temperature and stress. A depth path is defined along the normal direction of the highest point to obtain the variations of temperature, thermoelastic power, and plastic dissipation power with depth, thereby distinguishing the action ranges of surface frictional heat and subsurface deformation dissipation.

3. RESULTS AND DISCUSSION

3.1. Surface Temperature and von Mises Stress

In the initial stage of dual-roughness contact, only a few higher asperities on the brake disc make real contact with asperities on the brake pad. Because the real contact area decreases sharply, each individual contact point carries a higher pressure under the same normal load, and the frictional heat-flux density per unit area increases rapidly. The maximum temperature on the brake-disc side reaches 1409.5 °C, and the high-temperature regions appear as discrete fragmented patches, indicating that local flash temperature is mainly governed by a limited number of contact patches. The maximum temperature on the brake-pad side reaches 1571.9 °C, significantly higher than that on the brake-disc

side, mainly because the pad material has lower thermal conductivity, the rough body is larger, and surface heat is more difficult to diffuse into deeper regions.

The von Mises stress is likewise concentrated in the asperity regions in direct contact. The brake-disc side reaches a peak value of 1079.4 MPa at approximately 102.5 μs, while the brake-pad side reaches a peak value of 1024.6 MPa at approximately 136 μs. After the peak values appear, high-temperature softening, local plastic flow, and contact reconstruction cause the stress to diffuse toward the surrounding regions and gradually release. Temperature hot spots and stress-concentration regions do not completely coincide, indicating that the mechanical response is dominated by contact load bearing and stress-wave propagation, whereas the temperature peak is also controlled by frictional-work accumulation, heat diffusion, and material softening. This spatiotemporal mismatch is an important basis for hot-spot formation and thermoelastic instability in the dual-roughness interface.

The temperature and stress sequences show that local high-temperature patches form rapidly during the initial braking stage. As friction proceeds, some asperities are flattened by thermal softening and plastic deformation, and new asperity peaks enter contact, causing the heat-source position to migrate continuously. The contact pressure is also redistributed as the patches are renewed. The resulting unsteady contact process causes the high-temperature and high-stress regions to become spatially mismatched and drives the interface response to gradually shift from being dominated by mechanical loading to strong thermo-mechanical coupling.

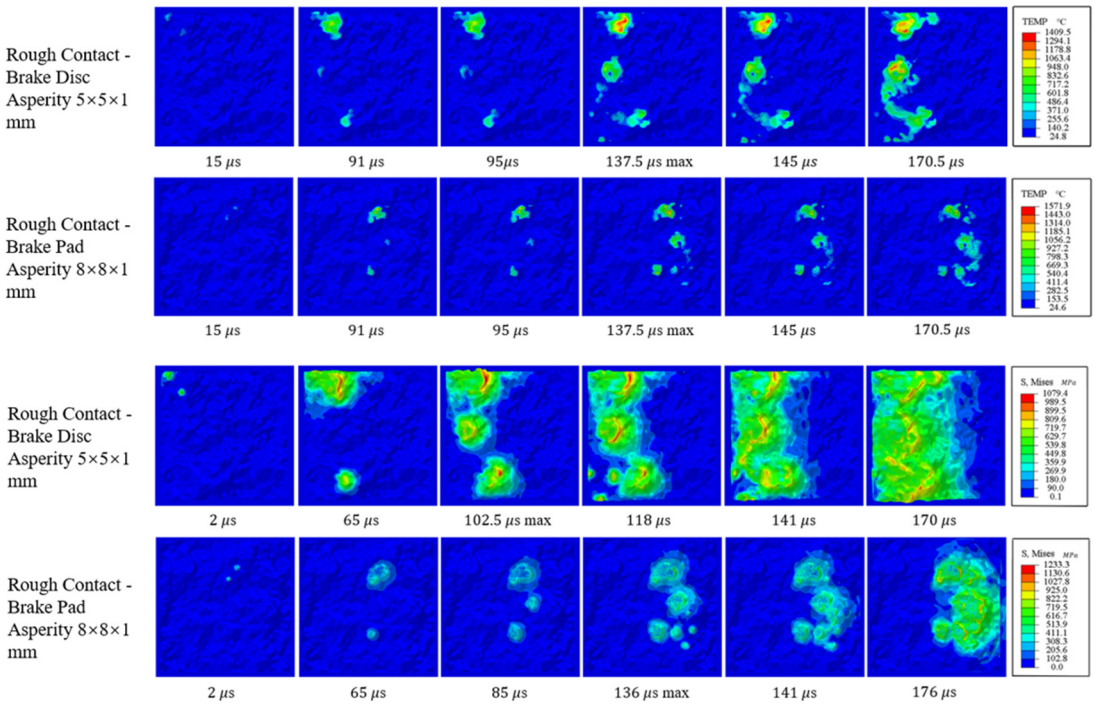

Figure 2. Temperature field and von Mises stress field under dual-roughness contact

3.2. Near-Surface Heat Accumulation and Heat Diffusion

Effective solid contact at the dual-roughness interface is borne by a small number of discrete patches. During compaction, sliding, and recontact of the asperities on both sides, the solid heat-transfer paths migrate continuously, while the microscopic gaps between patches increase the equivalent interfacial thermal resistance. Therefore, even if the total frictional work remains unchanged, heat is still concentrated in limited contact patches, forming a highly nonuniform surface temperature field.

The temperature distribution along the normal direction of the highest asperity shows that heat in the brake disc is mainly concentrated within a depth range of 0-0.05 mm, and the maximum thermal influence depth is approximately 0.389 mm. The high-temperature layer in the brake pad is mainly

concentrated in the 0-0.1 mm near-surface layer, and the maximum thermal influence depth is approximately 0.63 mm. Although the brake pad has a larger thermal influence depth, most heat still remains in the near-surface layer, indicating that lower thermal conductivity and rough-interface thermal resistance jointly cause significant heat accumulation.

The combination of high peak temperature and limited thermal influence depth manifests as "high surface temperature and rapid attenuation in deeper layers." This occurs because, after the asperities on both sides become misaligned, the continuous solid-solid heat-transfer path is divided into multiple small patches, and the gaps between patches form additional thermal resistance, suppressing heat diffusion along the thickness direction. The simultaneous increase in local heat-source intensity and decrease in overall heat-dissipation capacity are important conditions for the formation of flash temperature and hot spots at the dual-roughness interface.

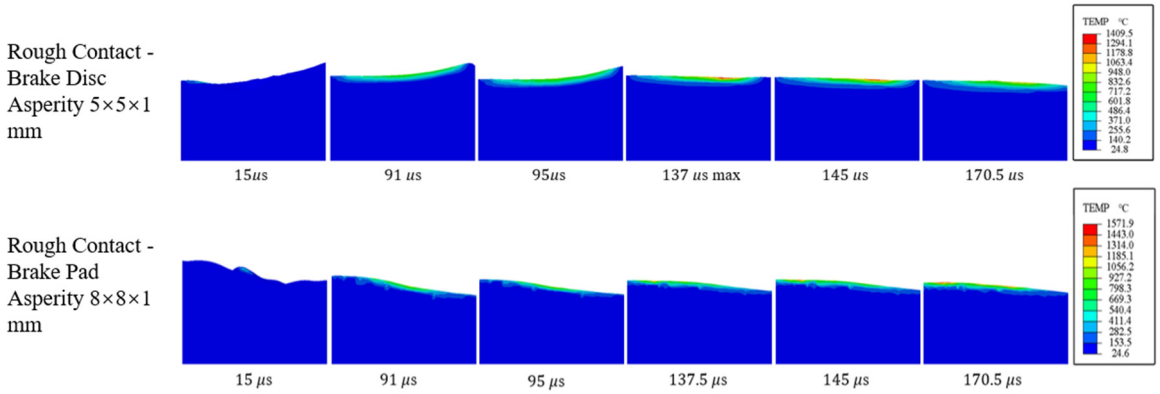

Figure 3. Cross-sectional temperature evolution of the brake disc and brake pad under dual-roughness contact

3.3. Thermoelastic Effects and Plastic Dissipation Depth

The depth wise distributions of thermoelastic-effect power and plastic dissipation power show that the two energy channels have distinctly different spatial scales. The influence depth of the thermoelastic effect can reach approximately 1.1 mm on the brake-disc side and approximately 1.9 mm on the brake-pad side, both of which are significantly deeper than the high-temperature region. This indicates that thermal expansion caused by rapid surface heating is not confined to the surface layer, but can propagate into the subsurface layer through elastic waves and strain coupling. For the brake disc, plastic dissipation is mainly concentrated in the extremely shallow surface layer of 0-0.075 mm, with a maximum influence depth of approximately 0.28 mm. For the brake pad, plastic dissipation is mainly concentrated within 0-0.22 mm, with a maximum influence depth of approximately 0.556 mm.

The power curves exhibit multiple peaks and oscillations, reflecting alternating load bearing, instantaneous separation, and decompaction of asperities during friction. Local high temperature reduces the material yield strength and drives the plastic zone to migrate toward deeper regions, while thermal softening and element damage weaken load-bearing capacity and limit the continued expansion of the plastic zone. The competition between these two effects makes energy conversion strongly time-dependent and spatially nonuniform.

The differences between the brake disc and the brake pad along the depth direction indicate that material properties modulate the energy-dissipation mode of dual-roughness contact. The brake disc has higher stiffness and better thermal conductivity, so its plastic dissipation zone is thinner but its stress peak is higher. The brake pad has lower stiffness and thermal conductivity, making the surface layer more susceptible to thermal softening and giving it a greater plastic-dissipation influence depth.

When the rough bodies on both sides deform synchronously, a joint shear zone spanning the contact interface can form near the interface, providing spatial conditions for synergistic plastic dissipation.

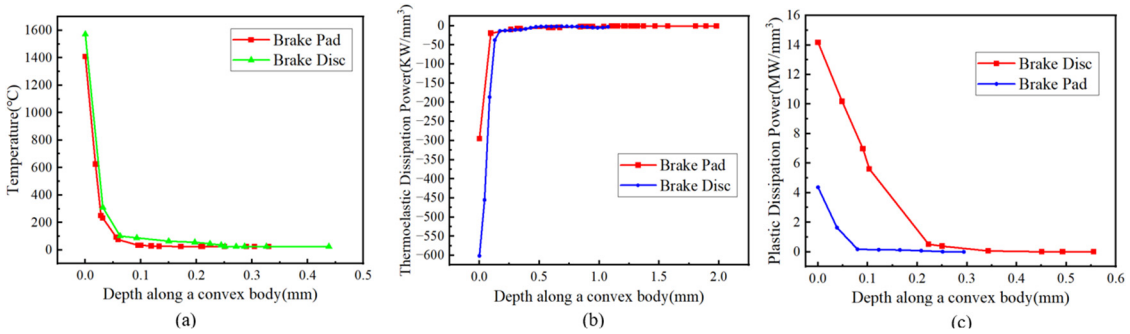

Figure 4. Distributions of temperature, thermoelastic power, and plastic power along asperity depth

3.4. Thermal-Instability Sequence and Frequency-Domain Characteristics

From the time-sequence perspective, the dual-roughness contact model exhibits the basic pattern that "the stress peak precedes the temperature peak." This phenomenon arises because the propagation speed of stress waves is much higher than that of heat diffusion. After friction begins, asperities first carry the local load and generate transient stress peaks. Subsequently, frictional work and plastic work are gradually converted into heat, the temperature rises rapidly and induces material softening, and the stress peak then decreases. The entire process can be divided into a mechanically dominated stage, a thermo-mechanically coupled stage, and a relaxation-equilibrium stage.

To quantify the intensity of stress oscillation, indicators such as relative oscillation amplitude, root-mean-square oscillation amplitude, and dominant frequency can be used:

$$A_{rel}=\frac{\sigma_{max}-\sigma_{min}}{\bar{\sigma}}\times 100\%,\quad A_{rms}=\sqrt{\frac{1}{N}\sum_{n=1}^{N}(\sigma[n]-\bar{\sigma})^2} \tag{10}$$

$$f_{dominant}=\underset{f\in[f_{\min},f_{\max}]}{argmax}[PSD(f)],\quad E_{total}=\sum_{k=0}^{N/2}PSD[k]\cdot\Delta f \tag{11}$$

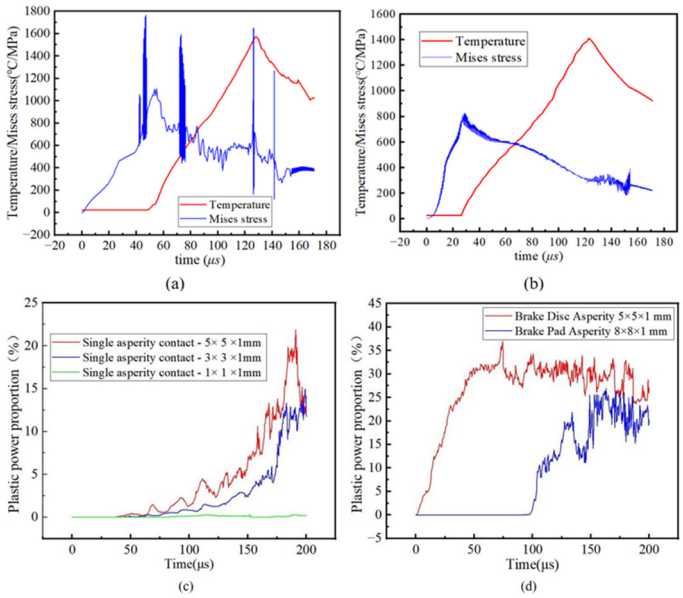

Figure 5. Temperature-stress time histories and energy power ratios under dual-roughness contact

After fast Fourier transform is applied to the von Mises stress time series, the dominant interfacial frequency is approximately 3395.6 Hz, and the relative oscillation amplitude is approximately 312.10%. This result indicates that direct collision of rough bodies causes continuous sudden changes in contact stiffness, and asperity compaction, separation, and recontact make the local stress fluctuate repeatedly in the high-frequency range. High-frequency instability promotes material fatigue and microcrack propagation and further intensifies the nonuniformity of the heat-flux distribution.

The frequency-domain characteristics can be explained by the height difference and phase difference between the asperities on both sides. Contact points are established and disappear frequently within a short time, causing the equivalent contact stiffness to jump repeatedly and producing broadband stress fluctuations and a pronounced dominant frequency. If this frequency approaches the structural natural frequency of braking components or the friction self-excited frequency, the vibration response may be further amplified. Therefore, interface morphology matching and contact-stiffness smoothing are important directions for suppressing dynamic instability.

3.5. Energy Distribution and Synergistic Plasticity Mechanism

The thermoelastic power alternates between positive and negative values around zero, indicating that this channel has the dual functions of "heat release" and "heat absorption." When the thermoelastic power is positive, elastic strain energy is released into heat and aggravates local temperature rise. When it is negative, the material expands rapidly due to instantaneous heating, and part of the heat is temporarily converted into mechanical strain energy, manifested as thermoelastic cooling or heat absorption. The positive-negative alternation of power oscillation reflects the rapid dynamic balance among mechanical energy input, heat accumulation, elastic work, and energy redistribution at microscopic contact points.

Plastic power characterizes the irreversible internal dissipation and damage accumulation of the material. In dual-roughness contact, the plastic power of the brake disc and the brake pad accounts for approximately 32% and 37% of the theoretical input power, respectively, indicating that a joint plastic zone spanning the scale of a single asperity is formed during mutual rolling and crushing of asperities on both sides, and that plastic deformation is jointly accommodated by the two materials. This synergistic plasticity mechanism can consume a relatively large amount of mechanical input energy, but it also intensifies surface damage, morphology reconstruction, and the risk of thermal instability.

From the perspective of energy management, a higher plastic-dissipation ratio does not necessarily indicate a safer braking state. On the one hand, plastic work can convert part of the mechanical energy into internal dissipation, reducing the proportion of energy input to the surface entirely in the form of interfacial frictional heat. On the other hand, plastic deformation causes irreversible material damage, surface morphology change, and contact-patch reconstruction, thereby affecting wear and hot-spot positions in subsequent braking cycles [1,8]. The high plastic ratio exhibited by the dual-roughness model suggests that the real braking interface may absorb a large amount of energy through material deformation, but if sufficient heat dissipation and stable contact area are lacking, this process may still evolve into thermal fatigue and local failure.

3.6. Engineering Implications

The dual-roughness contact model shows that interface design should not merely pursue a reduction in the roughness of one surface; instead, it should also consider the matching relationship between asperity peaks on the brake disc and brake pad. If the peak-valley height difference between the two surfaces is too large, the real contact area will decrease further, and both the local heat-flux density and stress oscillation will increase. If the surface is overly smooth, friction stability and running-in capacity may be weakened. Therefore, reasonably controlling asperity height, wavelength, and

distribution so that the number of contact patches is moderate and the heat-transfer paths are continuous is an important direction for suppressing local flash temperature.

In terms of materials, improving the thermal conductivity of the brake pad and optimizing the proportions of conductive and reinforcing components in the copper-based powder metallurgy material can reduce surface-layer heat retention. At the same time, excessively rapid high-temperature softening should be avoided; otherwise, the plastic zone will expand and contact-stiffness fluctuations will be induced. In terms of structure, heat-diffusion paths can be improved through pad segmentation, grooves, debris-removal features, and heat-dissipation channel design. For high-speed train brakes, the temperature, stress, frequency, and energy-ratio indicators provided by the dual-roughness model can serve as evaluation parameters for interface optimization.

Table 2. Key response indicators for dual-roughness contact

Component	Maximum temperature/°C	Peak von Mises stress/MPa	Thermal influence depth/mm	Thermoelastic depth/mm	Plastic power ratio
Brake disc	1409.5	1079.4	0.389	1.1	Approx. 32%
Brake pad	1571.9	1024.6	0.630	1.9	Approx. 37%

4. CONCLUSION

(1) Dual-roughness contact significantly reduces the real contact area and increases the local heat-flux density. The maximum temperatures of the brake disc and brake pad reach 1409.5 °C and 1571.9 °C, respectively, and the high-temperature regions appear as discrete patches. Because of its lower thermal conductivity and larger surface thermal resistance, the brake pad exhibits stronger heat accumulation.

(2) The peak von Mises stresses of the brake disc and brake pad are 1079.4 MPa and 1024.6 MPa, respectively, and the stress response precedes the temperature response. Continuous asperity collision, separation, and sudden changes in contact stiffness cause high-frequency interfacial instability at approximately 3395.6 Hz, with a relative oscillation amplitude of approximately 312.10%.

(3) Frictional heat is mainly retained in the shallow surface layer within 0.1 mm. The thermoelastic response can propagate into deeper subsurface regions, whereas plastic dissipation is concentrated near the surface. The plastic power of the brake disc and brake pad accounts for approximately 32% and 37% of the theoretical input power, respectively, confirming the existence of a synergistic plastic dissipation mechanism at the dual-roughness interface.

(4) From the perspective of engineering optimization, reducing the height difference between asperities on both sides, increasing the effective real contact area, improving the thermal conductivity of the brake pad, and weakening sudden changes in contact stiffness are potential directions for suppressing local flash temperature, high-frequency oscillation, and thermal instability. Future research should further introduce temperature-dependent friction coefficients, variations in material thermal properties, and measured random roughness, and should validate the dual-roughness model through experiments.

REFERENCES

[1] Lu, C., Yin, J. B., Mo, J. L., & Wang, J. Y. (2022). Accumulated wear degradation prediction of railway friction block considering the evolution of contact status. *Wear*, 494–495, 204251. https://doi.org/10.1016/ j.wear. 2022. 204251.

[2] Bowden, F. P., & Tabor, D. (1951). *The friction and lubrication of solids*. Oxford University Press.

[3] Sofuoglu, H., & Ozer, A. (2008). Thermomechanical analysis of elastoplastic medium in sliding contact with fractal surface. *Tribology International*, 41(8), 783–796. https://doi.org/10.1016/j.triboint.2007.12.003.

[4] Meng, D. J., Li, B. R., Zhang, L. J., Li, W. B., & Wu, J. F. (2024). Research on the evolution of friction hot spots in vehicle disc brake during braking based on experiment. *International Journal of Thermal Sciences*, 203, 109126. https://doi.org/10.1016/j.ijthermalsci.2024.109126.

[5] Chen, K., Wang, L. B., Chen, Y. G., & Wang, Q. W. (2017). Molecular dynamics simulation of microstructure evolution and heat dissipation of nanoscale friction. *International Journal of Heat and Mass Transfer*, 109, 293–301. https://doi.org/10.1016/j.ijheatmasstransfer.2017.02.046.

[6] Waddad, Y., Magnier, V., Dufrenoy, P., & De Saxce, G. (2019). Heat partition and surface temperature in sliding contact systems of rough surfaces. *International Journal of Heat and Mass Transfer*, 137, 1167–1182. https://doi.org/10.1016/j.ijheatmasstransfer.2019.03.120.

[7] Kim, Y., Sergey, K., Kim, H., Choi, K., & Lee, M. G. (2023). Residual stress development and thermo-elasto-plastic distortion in brake discs. *Tribology International*, 190, 109056. https://doi.org/10.1016/j.triboint.2023.109056.

[8] Mao, J. J., Ke, L. L., Yang, J., Kitipornvhai, S., & Wang, Y. S. (2017). Thermoelastic instability of functionally graded coating with arbitrarily varying properties considering contact resistance and frictional heat. *Applied Mathematical Modelling*, 43, 521–537. https://doi.org/10.1016/j.apm.2016.10.041.